ESC-TR-91-179

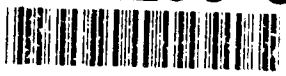

Technical Report
954

Real-Time Ionospheric Monitoring System Using the GPS

A.J. Coster
E.M. Gaposchkin
L.E. Thornton

24 August 1992

Lincoln Laboratory
MASSACHUSETTS INSTITUTE OF TECHNOLOGY
LEXINGTON, MASSACHUSETTS

Prepared for the Department of the Air Force
under Contract F19628-90-C-0002.

This report is based on studies performed at Lincoln Laboratory, a center for research operated by Massachusetts Institute of Technology. The work was sponsored by the Department of the Air Force under Contract F19628-90-C-0002.

The ESC Public Affairs Office has reviewed this report, and it is releasable to the National Technical Information Service, where it will be available to the general public, including foreign nationals.

This technical report has been reviewed and is approved for publication.

FOR THE COMMANDER

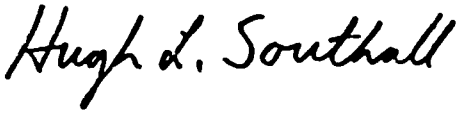

Hugh L. Southall, Lt. Col., USAF
Chief, ESC Lincoln Laboratory Project Office

MASSACHUSETTS INSTITUTE OF TECHNOLOGY
LINCOLN LABORATORY

REAL-TIME IONOSPHERIC MONITORING SYSTEM USING THE GPS

A.J. COSTER
E.M. GAPOSCHKIN
L.E. THORNTON
Group 91

TECHNICAL REPORT 954

24 AUGUST 1992

LEXINGTON MASSACHUSETTS

ABSTRACT

In satellite tracking using ground-based radars, an estimate of the total electron content (TEC) along the path to the satellite is required to measure accurately the range of the satellite. This estimate is necessary because the radar wave travels at a slower speed as it propagates through the ionosphere. The range error ΔR that is introduced is dependent on the radar frequency f and on the TEC along the propagation path, and can be expressed by

$$\Delta R\,(\text{meters}) = \frac{40.3}{f^2}\int_0^R N_e\,dr \quad , \tag{1}$$

where N_e is the local electron density and R is the radar range. The TEC can vary significantly with the time of day, geomagnetic activity, and look direction. A real-time synoptic ionospheric monitoring system has been developed using data acquired from a TI4100 Global Positioning System (GPS) receiver for use at the Millstone Hill satellite-tracking radar. The TI4100 GPS receiver can track up to four GPS satellites at any one time. Each GPS satellite transmits signals at two different L-band frequencies: L1 (1575.42 MHz) and L2 (1227.6 MHz). The TEC along the path to each satellite can be determined by combining both frequencies using the pseudorange and the integrated phase data. At Millstone, the TEC is measured every 3 s for each GPS satellite in view. The data are input into a Kalman filter that is used to predict the coefficients of a simple TEC model with azimuth and elevation dependence. This model takes advantage of the real-time knowledge provided by the GPS data of the variations in TEC around the Millstone location. The coefficients for this model are then sent to the satellite-tracking computer, and the model is applied in real time to account for the ionospheric path delay to whatever satellite is currently in track. The preliminary results of using this ionospheric monitoring system at Millstone will be discussed. The zenith value of the TEC predicted by our GPS model will be compared with another ionospheric measurement, the foF2 obtained from the collocated University of Lowell Digisonde. The TEC values predicted by our GPS model during both geomagnetically quiet and disturbed time periods will be discussed, as well as those associated with high solar flux time periods. Finally, the improvement in our radar system calibration due to the use of the new GPS model will be demonstrated. This improvement is evident in observations of the average range residual over a pass of the Lageos satellite. The standard deviation of these residuals drops from approximately 20 TEC units to about 5 TEC units when the new GPS model is used to estimate the ionospheric refraction correction. A TEC unit is 10^{16} electrons/m^2. At the Millstone radar frequency of 1295 MHz, this correction corresponds to an improvement in the standard deviation from 5.3 to 1.4 m. It is our opinion that, other than upgrading all satellite-tracking radars to dual-frequency capability, the GPS is currently the best monitoring system of the TEC available.

ACKNOWLEDGMENTS

We would like to thank Pat Doherty and J.A. Klobuchar for use of their Hamilton Faraday rotation data, and the University of Lowell for their foF2 information from the Digisonde. Michael Buonsanto and David Tetenbaum of the MIT Haystack Observatory, Atmospheric Sciences Group, provided the incoherent scatter data given here.

In addition, several of the computer-generated plots here were produced by Karl P. Buchmann.

TABLE OF CONTENTS

LIST OF ILLUSTRATIONS

1. INTRODUCTION

A transportable device has been developed at Lincoln Laboratory that uses the Global Positioning System (GPS) to determine real-time ionospheric path delays for use in satellite tracking. This system was integrated into the Millstone Hill real-time satellite-tracking software in March 1991. This report will present the initial satellite-tracking results using this system and will describe the Kalman filter used in obtaining the model coefficients. Before discussing the real-time data processing involved, some background information will be presented on both the ionospheric path delay and on the design and use of the GPS. This material will illustrate the importance of correctly estimating the ionospheric path delay and will explain how the GPS data can be used to determine it.

The ionospheric path delay is a consequence of the slower group velocity v_{gr} of the radar wave as it travels through the ionosphere. Therefore, the true range to the satellite R_t is somewhat less than the apparent range R_a, which assumed that the radar wave traveled at the speed of light c in a vacuum.

$$\Delta R = R_a - R_t = ct - v_{gr}t \quad . \tag{2}$$

The error in the measurement of radar range ΔR is dependent on the radar frequency f and the total electron content (TEC) along the ray path from the radar to the satellite. It can be expressed by the following equation:

$$\Delta R\,(\text{meters}) = \frac{40.3}{f^2}\int_0^R N_e\,dr \quad , \tag{3}$$

where N_e is the local electron density, and the integrated value of it is the TEC. The TEC can vary with look angle, time of day, season, geomagnetic activity, and solar flux value. Typical errors at L-band frequencies in radar range due to the ionosphere are about 32 m at 20 deg of elevation. At UHF frequencies, errors are estimated to be 280 m at 20 deg of elevation, nearly 10 times larger than at L-band.

The GPS design included the broadcast of two different frequencies so that the ionospheric delay term could be eliminated. Each GPS satellite is broadcasting a signal at L1 (1575.42 MHz) and at L2 (1227.6 MHz). By computing the difference in delay of the L1 and L2 signals, the ionospheric term can be computed directly. In practice, there is also the additional problem of multipath.

Unlike most GPS users, we do not consider the ionospheric delay term to be noise. Rather, we are using the GPS to measure the ionospheric TEC along the path to each GPS satellite in view. The Millstone GPS Real-Time Ionospheric Mapping System (GRIMS) [1] monitors the local ionosphere by continuously sampling both L-band frequencies for each satellite in view. The group delay and reconstructed carrier waves are then used to construct the TEC. By combining the TEC measurements from all satellites, a four-dimensional model (space and time) of the ionosphere is

generated. The coefficients of this model are then sent to our satellite-tracking computer and are used in real time to compute the ionospheric correction in the direction that the Millstone radar is pointing.

All results presented here are given in TEC units, the number of electrons x $10^{16}/m^2$. For easy reference, 1 m of range correction at L1 = 6.15929 TEC units. 1 TEC unit = 2.85 x TDD, where TDD is equal to TTL2 –TTL1 (transit time of L2 – transit time of L1 in ns), and stands for time of differential delay.

2. GPS TEC MEASUREMENTS

In principle, the ionospheric path delay can be obtained directly from the difference in the GPS pseudorange measurements. However, although the GPS group delay measurements are accurate enough for the majority of user needs, the ionospheric correction cannot be determined directly from this data. This effect is due primarily to multipath and the L1/L2 biases.

Multipath effects in the group delay data account for approximately a 6-ns increase in the noise level. For comparison, a 2-ns increase in group delay amounts to a 1-m error in the path delay at L-band. At Millstone, the multipath effects have been reduced by the use of absorbing material under the GPS antenna and can be further reduced by data averaging [2]. The multipath problem is not as severe in the GPS integrated phase measurements. The GPS phase data show an increase in the noise level on the order of only 50 ps [3]. The trouble with the phase data is that it contains an unknown bias due to the integer cycle ambiguity of phase measurements (i.e., the number of full phase cycles between the satellite and receiver is not known). By combining the GPS integrated phase data with the group delay data, the difficulties inherent with both data types may be overcome.

Figure 1 illustrates both the GPS integrated phase and GPS group delay data plotted as a function of time for one satellite (SSC number 11054, PRN number 6) that was in view from Millstone during a 3-h time span in March 1989. The increased noise level due to multipath is apparent in the group delay data. The smooth appearance of the integrated phase data shows that it is less susceptible to multipath. To account for the unknown cycle ambiguity and bias, the mean value of the phase data is set equal to the mean value of the group delay data.

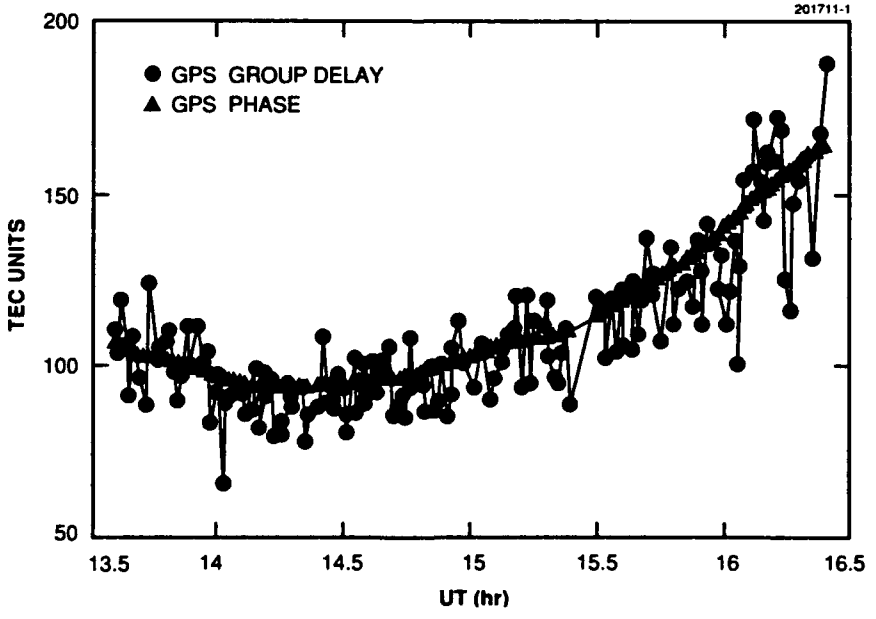

Figure 1. Illustration of GPS phase and group delay data. Satellite SSC no. 11054, PRN no. 6, 1 March 1989.

Another problem with making TEC measurements using GPS data is that both the satellite and the receiver hardware introduce an unknown bias—or additional delay—between the L1 and L2 signals. These biases must be measured or estimated and removed from the GPS group delay data in order to determine accurately the ionospheric path delay. These biases have been studied extensively [3–6].

Coco et al. [5] have shown that although the TI4100 receiver (the GPS receiver used at Millstone) bias varies from unit to unit, the change over time in the bias is quite small. They estimated the day-to-day variation of the TI4100 bias over a five-week period to be less than 0.5 ns (corresponding to a 23-cm effect at L1 or 1.4 TEC units). The Millstone TI4100 GPS receiver is assumed to have a negligible bias because, at times, the difference between the Millstone GPS TEC measurements and those of the collocated incoherent scatter (IS) radar has been measured to be less than 1 TEC unit (0.35 ns of differential delay).

Satellite biases are more difficult to determine and pose a serious problem to ionospheric estimation when using the GPS. Studies have developed techniques for determining the space vehicle (SV) biases using a multistation system of receivers [3,4]. The JPL-determined biases [7] have been adopted for the work reported here, as this is the standard convention in the ionospheric community.

In Figure 2, a comparison of GPS, incoherent scatter, and Hamilton TEC measurements is shown. The measurements were taken on 27 April 1990. The GPS receiver at Millstone was tracking the GPS satellite PRN number 6 while it was in view. At the same time, the Millstone UHF IS radar was pointed so that it was taking IS measurements of the ionosphere along the same line of sight to this GPS satellite. The IS data were then processed to give an alternate determination of the TEC [8]. The IS data were carefully calibrated at the beginning and end of each run using foF2 data from a collocated Digisonde that was operated by the University of Lowell. The Millstone UHF radar can provide electron density profiles from approximately 100 to 1000 km or higher. Due to the decreasing signal-to-noise ratio, however, data at altitudes above 800 km have been eliminated here. The IS TEC measurements presented in this plot have been derived by integrating the electron density profiles from 100 to 800 km in height.

Figure 2 also shows a comparison of our GPS data with the TEC data taken at Hamilton, Massachusetts. Using the technique of Faraday rotation, the polarimeter at Hamilton measures the change in phase of a signal transmitted by the GOES-B satellite. The Faraday rotation technique measures the TEC up to approximately 2500 km [7], due to the smaller magnetic field at higher altitudes. GOES-B is at a range of approximately 39,000 km. Because Hamilton is at nearly the same latitude and at a comparable longitude to Millstone, our GPS measurements of TEC can be compared to Hamilton's measurements as long as our measurements are made looking along a similar line of sight (LOS) to that of Hamilton's LOS to GOES-B. The comparison shown in Figure 2 has made some adjustment for the different elevations of the GPS and Hamilton measurements. The difference between the Hamilton and GPS TEC data is less than 2 TEC units. Basically, Figure 2 compares the GPS measurement of TEC out to 19,000 km, the Faraday rotation measurement out to 2500 km, and the IS measurement of TEC out to 800 km. The large difference between the IS measurements of TEC and the Hamilton and the GPS measurements of TEC can be attributed to the

fact that the ionosphere extends significantly above 800 km during time periods of high solar flux. In April 1990, the F10.7 cm flux was more than 200. Further information on TEC observations detected above 800 km can be found in associated literature [9].

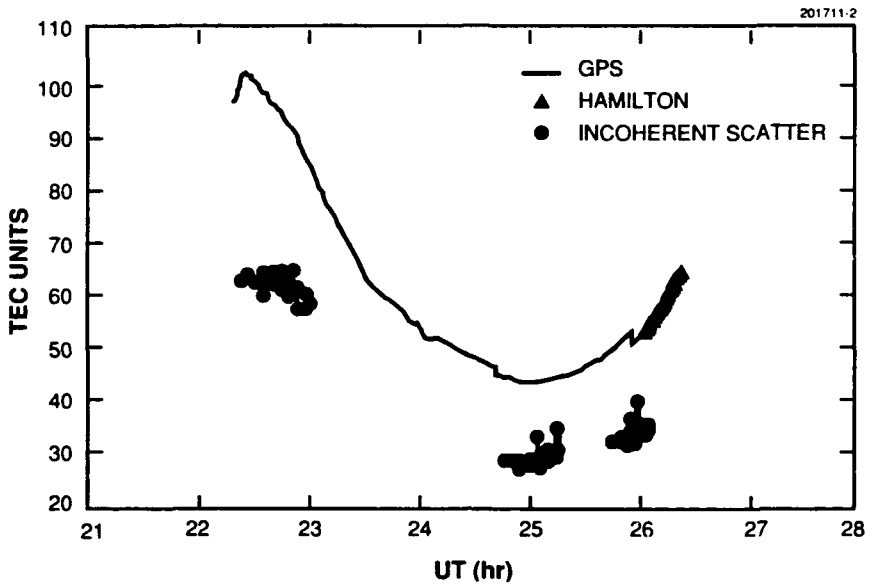

Figure 2. Comparison of GPS, incoherent scatter, and Hamilton TEC measurements. GPS Satellite SSC no. 11054, PRN no. 6, 27 April 1990.

3. GPS PREPROCESSING

The GPS data is preprocessed before it is sent to the Kalman filter. This preprocessing includes reconstructing the L1 and L2 SV times, applying the SV clock corrections, and fixing detected cycle slips in the integrated phase data. The algorithms used in the preprocessing are described here.

The TI4100 GPS receiver acquires the GPS data. Then, in the preprocessing, the raw L1 and L2 SV times are reconstructed, and the space vehicle (SV) clock corrections are applied. The SV clock correction is given by

$$\Delta t_{sv} = a_{f0} + a_{f1}\left(t - t_{oc}\right) + a_{f2}\left(t - t_{oc}\right)^2 + \Delta t_r \quad , \tag{4}$$

where

Δt_{sv} = the satellite (SV) clock correction (s),

a_{f0} = polynomial coefficient (s),

a_{f1} = polynomial coefficient (s/s),

a_{f2} = polynomial coefficient (s/s^2),

t = GPS system time (s),

t_{oc} = clock data reference time (s),

Δt_r = relativistic correction term (s).

In addition,

$$\Delta t_r = -\frac{2RV}{c^2} \quad , \tag{5}$$

where

R = instantaneous position vector of the SV (m),

V = instantaneous velocity vector of the SV (m/s),

c = speed of light (m/s).

The navigation (NAV) data are used to calculate the azimuth and elevation for each data point.

Sometimes the GPS receiver loses lock on a satellite. When this happens, the receiver loses track of the phase front cycle count for the satellite in question. This condition is called a cycle slip. To correct for cycle slips, the phase range, pseudorange, and SV time data are entered into a routine that tests for (and, if necessary, fixes) cycle slips.

The algorithm used for fixing cycle slips is based on the JPL GPS data-editing algorithm described by Blewitt [10]. This method has the important advantage that it can be implemented in real time. The technique uses linear combinations of the recorded carrier phases and the P code

pseudoranges to compute a wide-lane bias. Jumps in the wide-lane bias indicate data outliers and cycle slips. Outliers are thrown out, and cycle slips are fixed by determining the integer offset between the data arcs before and after the cycle slip.

The linear combinations of the phase and pseudorange residuals were found to be the most useful in our system. The routine implemented by the TI4100 process uses these data to determine whether a cycle slip has occurred. When two consecutive measurements for an SV indicate the presence of a cycle slip, then the algorithm attempts to correct the cycle slip.

If the measurements are accepted by the cycle slip algorithm, then the azimuth, elevation, and range are computed from the ephemeris. Range residuals are produced for both the phase and pseudorange data.

The measurements that pass the cycle slip test are then passed on to the Kalman filter sequential estimator routines. The filter uses as input the fractional part L1 and L2 SV times (in seconds), the x-y-z position, and the L1 and L2 phase ranges for a single satellite. The Kalman filter estimates the current filter state of the six coefficients that represent the local ionosphere. The model is described in the next section. The Kalman filter employs a fading memory mechanism that ensures that the most recent data are weighted more heavily than older data. In addition, a second cycle-slip test is applied by the Kalman filter.

4. GPS REAL-TIME MODEL

The model of the ionosphere used in our real-time GPS system has two components: a vertical TEC, which depends on both azimuth and elevation from the site, and a mapping function, which depends on elevation and range. The mapping function translates the vertical TEC value into a TEC value that is valid along the line of sight. This mapping function is described in Appendix A. In solving for the vertical TEC term, six coefficients are estimated, a_0 through a_5. These six coefficients are the parameters that define the ionosphere around the Millstone location. The model for the zenith correction has a center point, or pole, defined at a 90° elevation. The pole corresponds to a zenith correction term a_0 that is the estimate for the ionospheric TEC directly above Millstone. All of the TEC measurements are used in calculating the zenith TEC value over Millstone. The area around the pole is then divided in azimuth into quintets. Separating each quintet is a line that represents the linear interpolation of the vertical TEC from an elevation equal to 90° down to 0°. These lines are defined by the following equation that depends on both the elevation and on the coefficients, a_i, $i = 0,...,5$.

$$\text{TEC(vertical)} = a_0 + a_i \left[\frac{(90° - EL)}{90°}\right]^2, i = 1,5 \quad . \tag{6}$$

These quintets represent five different azimuth regions of the ionosphere around Millstone, as seen in Figure 3.

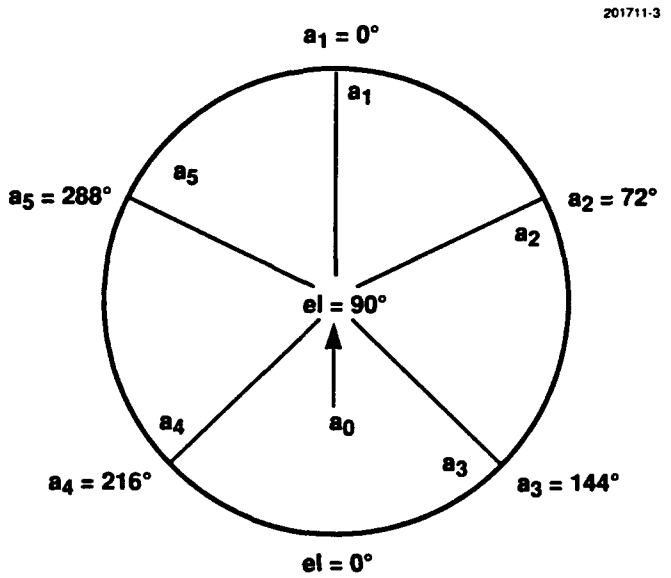

Figure 3. Circus Tent model of ionosphere around Millstone location.

The center of Figure 3 corresponds to a 90° elevation above Millstone; however, the rim of the circle is at a 0° elevation. The pole a_0 that is at a 90° elevation, represents our estimate of the TEC directly above Millstone. The zero azimuth (a_1) relative to this model is offset from the geographical 0° azimuth by 346° to align the relative coordinate system with the geomagnetic north pole. This alignment was done because geomagnetic coordinates provide a more natural system of describing the ionosphere. For example, an electron density trough forms frequently at night toward the north from Millstone, and this trough tends to align itself around the geomagnetic north pole.

The advantage of this parameterization of the ionosphere is that it preserves the azimuth and elevation information that is available from the different GPS satellites in view. If no GPS satellite is in view in either of the two neighboring quintets, then the a_0 value is used to estimate the TEC in that direction. In the real-time satellite-tracking program, a linear interpolation in azimuth between two neighboring lines is used to compute the best estimate of the TEC along the line of sight to the satellite. For example,

$$\begin{aligned}\text{TEC(vertical)} = W * \left(a_0 + a_i \left[\frac{(90° - EL)}{90°} \right]^2 \right) \\ + (1 - W) * \left(a_0 + a_{i+1} \left[\frac{(90° - EL)}{90°} \right]^2 \right) ,\end{aligned} \tag{7}$$

where W is a linear weighting factor, and $i = 1, 5$.

Kalman filters are discussed in detail by Jazwinski [11]. The specific filter used in our GPS ion model is described in Appendix B. The coefficients a_i, $i = 0,...,5$ (defined as the filter state) are estimated in the Kalman filtering process. The observations that map into the estimation of the filter state are the individual TEC measurements and their corresponding azimuths and elevations. One set of measurements exist for each satellite in view at any given time. For example, if four satellites were viewed at time t_0, then there will be four observations of the TEC, plus their associated azimuths and elevations, that will be used to compute that particular filter state along with all past measurements of TEC that have been appropriately age-weighted. The TEC measurements used are the combined pseudorange and integrated phase measurements.

Figures 4(a), (b), and (c) show a comparison of the vertical TEC values above Millstone as a function of the time of day. Figure 4(a) shows the vertical TEC predicted by our real-time GPS model. Figure 4(b) shows the TEC values predicted by the Bent ionospheric model. Figure 4(c) shows the TEC values predicted by the Slab model of the ionosphere [12], combined with a real-time measurement of the foF2. The Slab model of the ionosphere, combined with the real-time foF2 information, is the "old" ion model used in the real-time satellite-tracking program at Millstone. As can be seen in these three figures, on average, the zenith values agree among the different models. The diurnal trend of the TEC is clearly evident, although the GPS model shows a slightly different behavior than the Bent and Slab models predict.

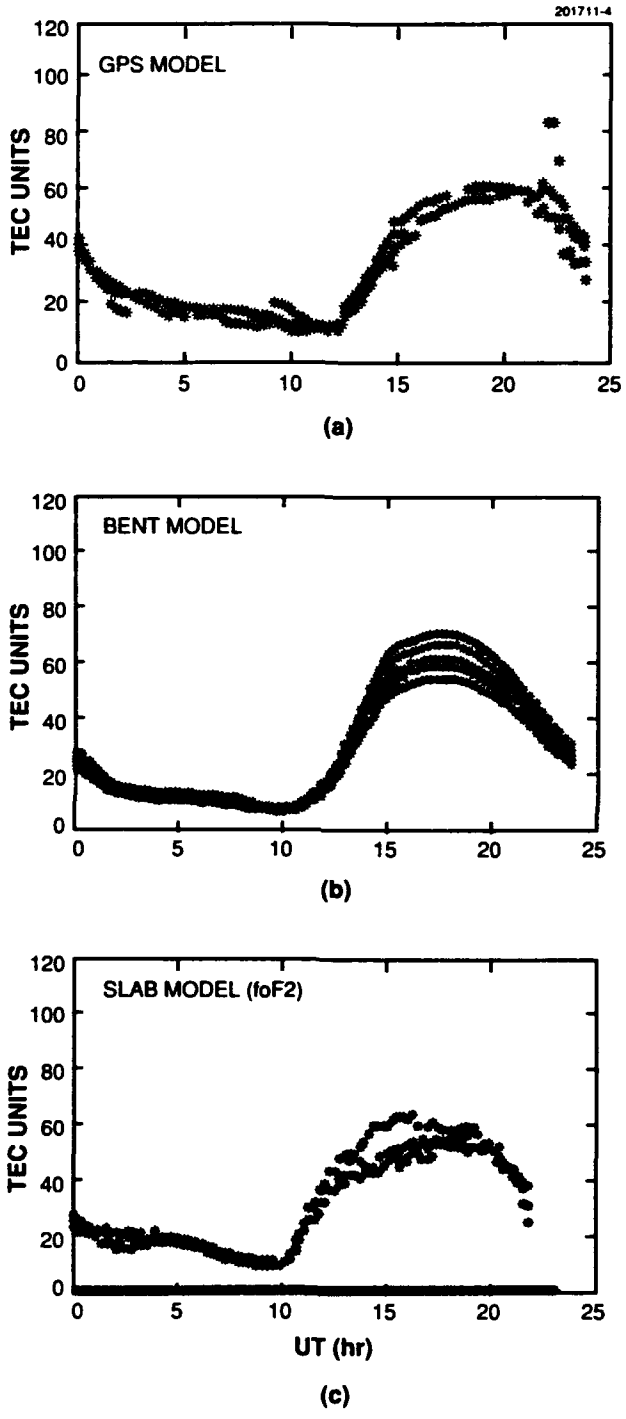

Figure 4. Zenith TEC model comparisons, 3–10 February 1991.

5. LAGEOS TRACKING

The Millstone radar tracks the Lageos satellite on a regular basis, nearly once a day. Lageos is a satellite with a perigee of approximately 5833 km and an eccentricity of 0.0047. Lageos is equipped with cube corner reflectors and thus can be tracked by NASA's laser ranging system. These lasers have a ranging accuracy of 10 cm or better.

The Lageos laser ranging data are used to monitor the calibration of the Millstone radar. Using an in-house orbit determination program called Dynamo [13] and the precision laser ranging data, the position of Lageos can be predicted to within 20 cm. By comparing our measured observations of Lageos with the predictions of Lageos, an estimate of the system bias in our radar can be determined. This procedure is followed at Millstone on a weekly basis, as radar calibration is an ongoing process.

When the real-time GPS ionospheric monitoring system was integrated into the satellite-tracking system last March, we frequently switched between the two methods of estimating the ionospheric correction: the new method that uses the GPS Kalman filter and the old method that uses real-time foF2 information combined with a Slab model of the ionosphere [12]. We then identified which Lageos passes used the new GPS ionospheric model and which used the previous ionospheric model to determine the ionospheric delay term. Figures 5(a) and (b) show the difference in the estimates of the average Lageos range bias for the two ionospheric models and for several of these passes.

Notice the difference in the size of the standard deviation between the data using the GPS ion model (5.94 TEC units) versus the data using the Slab model (22.02 TEC units). Clearly, the GPS ion model represents a significant improvement in our ionospheric correction estimate. Interestingly, the residuals that use the old ion model in Figure 5(b) seem to improve during the latter half of the year. This improvement occurs partially because fewer passes were taken using the old ion model and partially because several of the passes contain at least some GPS data. To qualify as being a GPS pass, more than 50% of the data in a pass had to have been taken using the GPS data to correct for the ionospheric term.

It is also worth observing that several of the Lageos passes were taken during geomagnetically disturbed time periods (defined here as having a daily A_p greater than 20). In fact, half of the Lageos passes taken using the GPS ion model qualify as "disturbed" time periods. It is extremely noteworthy that there is no evidence in the residuals of which days were geomagnetically disturbed.

One last figure is presented that shows the dramatic difference in the prediction of the ionospheric range correction between the GPS model and the old ion model used at Millstone. The data were taken on 20 July 1991, a day when the daily A_p was 32 and, in fact, the A_p had been elevated for the entire prior week. In Figure 6, the ionospheric range correction estimated by both the GPS model and the Slab ion model is shown over an entire pass of Lageos. The GPS model predicts a range correction that is noticeably less than the old ion model, particularly at the beginning of the pass that corresponds to low elevation data. The Lageos range residual that was calculated using

the GPS estimate of the ionospheric correction, is the bottom line on the axis. The Lageos range residual remains close to zero during the entire pass. This residual clearly indicates that the GPS estimate of the range correction is correct and is a significantly better estimate of the true ionospheric correction than that of the previous model.

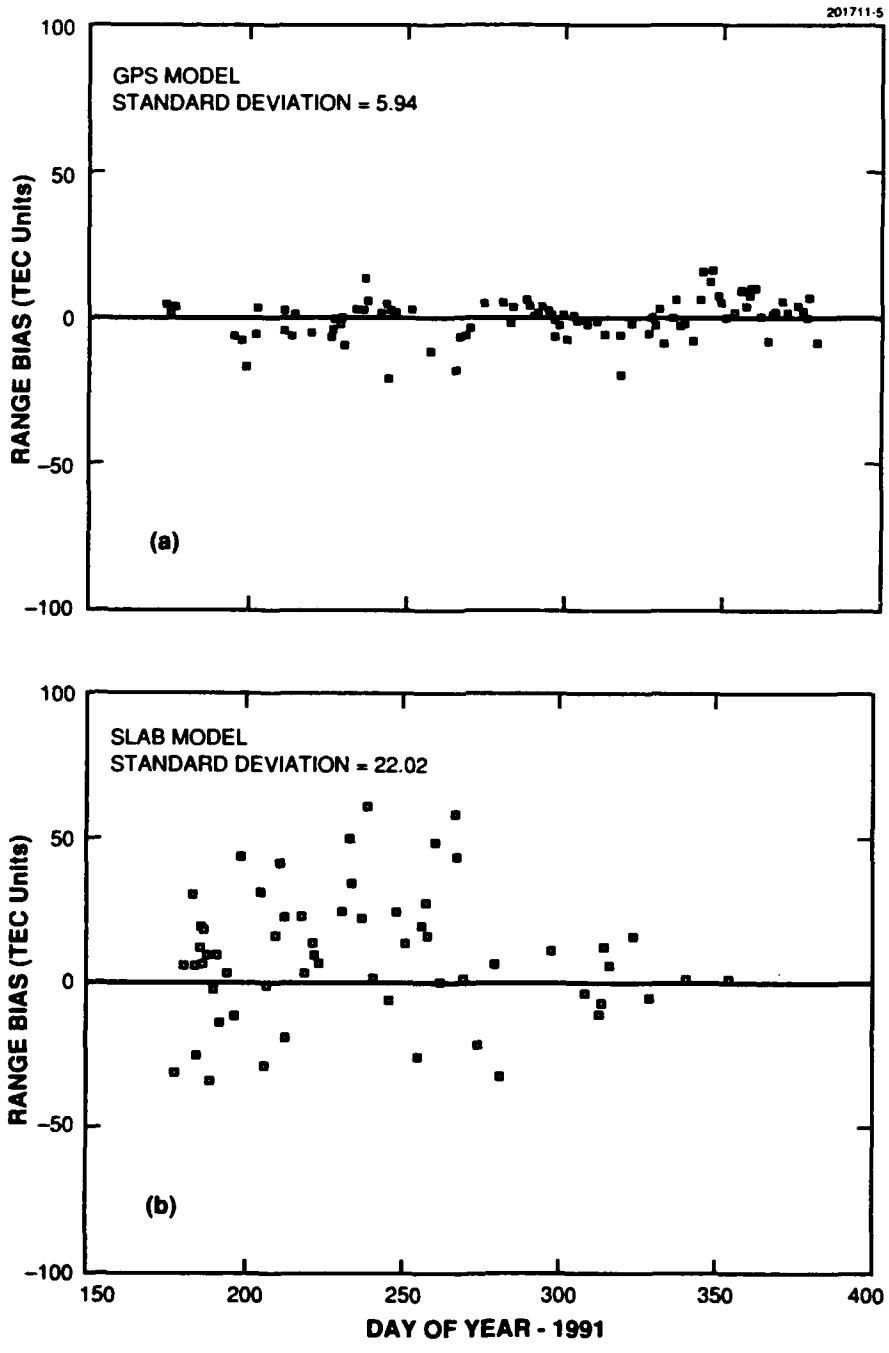

Figure 5. (a) Lageos residual using GPS ion model. Standard deviation = 5.94 TEC units. (b) Lageos residual using old ion model. Standard deviation = 22.02 TEC units.

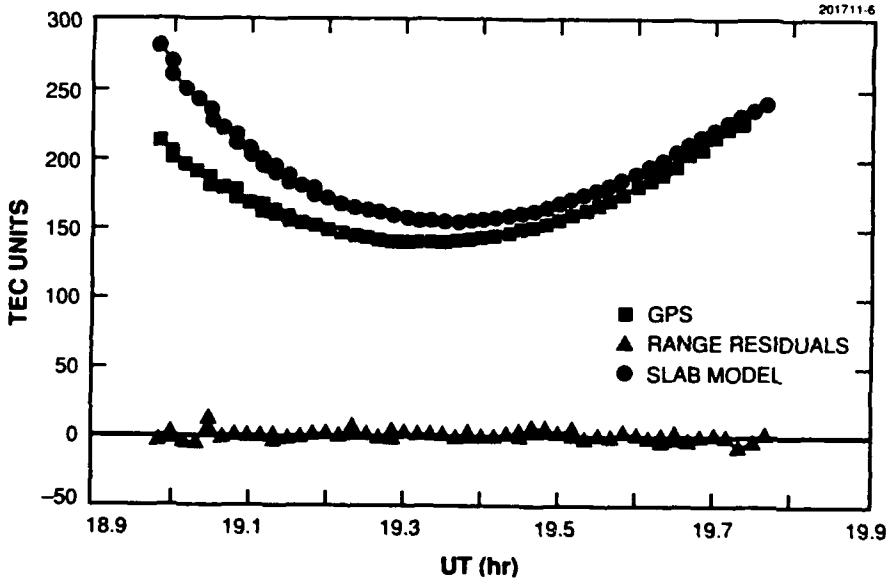

Figure 6. Lageos range bias versus refraction corrections: GPS and old ion model estimates, 20 July 1991.

6. CONCLUSION

A real-time ionospheric monitoring system has been developed and integrated into the Millstone Hill satellite-tracking operation. Initial results clearly indicate significant improvement in the estimation of the ionospheric delay term.

APPENDIX A
IONOSPHERIC MAPPING FUNCTION

The mapping function is used to transform the zenith or vertical path delay or TEC to an arbitrary zenith distance. The model assumes a spherically stratified ionosphere with a simple height distribution of electrons. The model is an extension of the Slab model, which is often used to interpret and apply ionosonde foF2 measurements to TEC estimates. The distribution of electrons is

$$N_e(h) = \begin{cases} 0 & h_{upper} < h \\ \dfrac{1}{1+\dfrac{h-h_{max}-S}{B}} & h_{max}+S < h < h_{upper} \\ 1 & h_{max} < h < h_{max}+S \\ \dfrac{1}{1+\dfrac{h_{max}-h}{A}} & h_{bottom} < h < h_{max} \\ 0 & h < h_{bottom} \end{cases} \quad , \qquad (A-1)$$

where

h_{max} is the lower boundary of the slab,

S is the thickness of the slab,

h_{upper} is the top of the ionosphere,

h_{bottom} is the bottom of the ionosphere, and

A and B describe the decay of the electron density from the center of the slab to the "bottom" and the "top" of the ionosphere, respectively. Nominal values can be h_{max} = 300 km, S = 200 km, h_{upper} = 1000 km, h_{bottom} = 100 km, A = 30 km, and B = 100 km. The model is normalized to a zenith TEC of 1, and the mapping function can be applied directly to calculate the TEC along a path at a given zenith distance and range. It can therefore be used to calculate the TEC or path delay to a point in the ionosphere.

The mapping function is formulated in terms of the zenith distance z, the range to the satellite from the observing station r, and the geocentric height of the station r_o. The height of the target h is calculated with

$$h = \sqrt{r_o^2 + r^2 + 2r_o r\cos(z)} - r_o \quad . \qquad (A\text{-}2)$$

Now the contribution from the slab is

$$Z_{slab} = \sqrt{\left(r_o + h_{max} + S\right)^2 - \left(r_o \sin(z)\right)^2} - \sqrt{\left(r_o + h_{max}\right)^2 - \left(r_o \sin(z)\right)^2} \quad . \qquad (A-3)$$

If the target height, $h_{max} < h < h_{max} + S$, then this contribution is evaluated with $S = h - h_{max}$. If $h < h_{max}$, there is no contribution from the slab.

The decay of electron charge from the slab depends on the parameters A and B. The integrals can be done analytically and are taken from Gradshteyn & Ryzhik [14], Equations 2.275.4, and 2.266. They are

$$I_{2.275}(a,b,l,u) = \int_l^u F(x)\,dx = \frac{l}{\sqrt{a}} \ln\left(\frac{u\sqrt{a} + \sqrt{u^2 - b^2}}{l\sqrt{a} + \sqrt{l^2 - b^2}}\right) \quad , \qquad (A-4)$$

and

$$I_{2.266}(a,b,l,u) = \int_l^u G(x)\,dx = -\frac{a}{c} \ln\left(\frac{l}{u} \frac{c^2 + au + \sqrt{c^2\left(c^2 + 2au + u^2\right)}}{c^2 + al + \sqrt{c^2\left(c^2 + 2al + \cdots\right)}}\right) \quad . \qquad (A-5)$$

The contribution from the lower ionosphere is

$$Z_{lower} = -A\left(I_{2.275}\left(1.0, r_o \sin(z), r_o + h_{max}, r_o + h_{bottom}\right)\right) + I_{2.266}\left(r_o + h_{max} + A, r_o \sin(z), -A, h_{bottom} - h_{max} - A\right) \quad . \qquad (A-6)$$

For the zenith $z = 0$,

$$Z_{lower}(z=0) = A \ln\left(\frac{h_{max} + A - h_{bottom}}{A}\right) \quad . \qquad (A-7)$$

The contribution from the upper ionosphere is

$$Z_{upper} = B\left(I_{2.275}\left(1.0, r_o \sin(z), r_o + h_{upper}, r_o + h_{max} + S\right)\right) + I_{2.266}\left(r_o + h_{max} + S - B, r_o \sin(z),\ h_{upper} - h_{max} - S + B, B\right) \quad . \qquad (A-8)$$

For the zenith $z = 0$,

$$Z_{upper}(z=0) = B \ln\left(\frac{h_{upper} - h_{max} - S_B}{B}\right) \quad . \qquad (A-9)$$

The limits of integration are adjusted in the obvious way for an object within the ionosphere.

Finally, the mapping function is normalized to the zenith using

$$Z(z,r) = \frac{Z_{slab}(z,r) + Z_{upper}(z,r) + Z_{lower}(z,r)}{Z_{slab}(0,\infty) + Z_{upper}(0,\infty) + Z_{lower}(0,\infty)} \quad . \qquad (A-10)$$

APPENDIX B
SEQUENTIAL ESTIMATOR OF THE CIRCUS TENT MODEL

The Circus Tent model of the ionosphere was designed specifically as a local model and follows traditional modeling by employing a mapping function. The parameterization also provides a comparison with other data (e.g., zenith path delay from an ionosonde). Six disposable parameters were chosen to correspond to the data available (i.e., a four-channel TI4100 GPS receiver).

The Circus Tent model represents the vertical total electron content (TEC) as a function of zenith distance ($z = 1/2\pi - \text{ele}$) and azimuth (Az). The half space centered at the station is divided into five equal pie-shaped sectors (quintets). The azimuth of the five sides are 346°, 58°, 130°, 202°, and 274°. These sectors orient the Circus Tent model along the natural magnetic coordinates of Millstone Hill. The TEC along a sector edge at Az_i is modeled as

$$\mathrm{TEC}\left(z, Az_i\right) = a_0 + a_i\left[\frac{z}{\pi/2}\right]^2 \quad . \tag{B-1}$$

The TEC is never allowed to be negative. The TEC at an arbitrary azimuth is obtained by linear interpolation as

$$\mathrm{TEC}(z, Az) = \mathrm{TEC}\left(z, Az_j\right) + \left[\mathrm{TEC}\left(z, Az_i\right) - \mathrm{TEC}\left(z, Az_j\right)\right]\frac{Az - Az_j}{2\pi/5} \quad , \tag{B-2}$$

where $Az_j < Az < Az_i$. Note that a_0 corresponds to the zenith TEC. The quadratic dependence of zenith distance was found to be a better model than a linear dependence. This is probably because the mapping function is very nearly linear and already models the ionosphere quite well.

Three separate steps are involved in the sequential estimate of the six model parameters that define the Kalman filter state. The first step is correcting possible cycle slips in the carrier phase data, which is in addition to the cycle slip corrections determined in the preprocessing, as described in Section 3. The second step is using the carrier phase to smooth the pseudorange. Finally, the third step is the prediction of the state at the observation time and the correction of the state using the observation vector.

CYCLE SLIP CORRECTION

The cycle slip correction models the carrier phase ϕ_{L1} and ϕ_{L2} as rational polynomials

$$\phi(x) = \frac{a_0 + a_1 x + a_2 x^2}{1 + a_3 x} \quad . \tag{B-3}$$

The existence of a cycle slip in L1 and L2 is tested as follows. First, the polynomial coefficients a_0, a_1, a_2, and a_3 are computed by least squares from the previous 20 measurements of carrier phase.

The first 20 observations in a sequence are assumed to be error free. The independent variable of the fit is centered and scaled to the data interval with

$$x_i = \frac{t_i - t_{\text{mid}}}{t_{\text{max}} - t_{\text{min}}} \quad , \tag{B-4}$$

where t_i is the observation time, t_{mid} is the average of all the times in the interval, t_{min} is the first time in the interval, and t_{max} is the last time in the interval. The L1 and L2 phases are then predicted for the next observation. The difference in predicted and observed phase for L1 and L2 are converted to cycles using 0.19029 m and 0.24421 m as the wavelengths. Then the difference in predicted phase is compared with the difference in observed phase. If the difference in phase difference exceeds 4.5 cm and integral cycle slips are predicted, a cycle slip is declared. The integral number of cycles, expressed in meters, is then added to all subsequent observations of L1 and L2 as appropriate. The cycle slip correction is cumulative. However, if three consecutive observations have a cycle slip or the number of cycles slipped exceeds 100, the process aborts. The phase accumulation and smoothing of pseudorange data for the particular satellite are then restarted.

PHASE SMOOTHED PSEUDORANGES

The difference in the observed pseudorange Δr, corrected for satellite and receiver bias (defined in Section 2), is a direct measurement of the TEC along the LOS to the satellite. The differences in the observed, cycle slip corrected, carrier phase, and $\Delta\phi$ (in meters) are different from the LOS TEC by a constant (i.e., the LOS TEC at the beginning of the set of data). Therefore, the smoothed data $\Delta\phi$ for the nth data point is taken as

$$\Delta\rho_n = \Delta\phi_n + \sum_{i=1}^{n}\left(\frac{\Delta r_i - \Delta\phi_i}{n}\right) \quad . \tag{B-5}$$

Some data screening is possible. First, a pseudorange difference or carrier phase difference that is negative or more than 50 m is declared an error, and the observation is skipped. Five consecutive errors cause the phase accumulation and smoothing of pseudorange data for a particular satellite to be restarted. In addition, for use in the Kalman sequential estimator, each observation has an associated uncertainty based on the standard error of fit and an observation noise of 0.20 m.

$$\sigma_n = \sqrt{\frac{\sum_{i=1}^{n}\left(\Delta r_i - \Delta\phi_i\right)^2}{n} - \left(\frac{\sum_{i=1}^{n}\Delta r_i - \Delta\phi_i}{n}\right)^2 + (0.20)^2} \quad . \tag{B-6}$$

SEQUENTIAL ESTIMATOR

The sequential estimator developed here follows Jazwinski's theoretical framework [11]. The sequential estimator processes the smoothed pseudorange data, corrected for satellite bias, as measurements of LOS TEC. The measurement **y** is a vector of up to four contemporaneous $\Delta\rho$'s

$$\mathbf{y} = \begin{bmatrix} \Delta\rho_1 \\ \Delta\rho_2 \\ \Delta\rho_3 \\ \Delta\rho_4 \end{bmatrix} \qquad (B-7)$$

from satellites 1, 2, 3, and 4. The data are used to estimate the ionospheric state x made up of the six Circus Tent parameters

$$\mathbf{x} = \begin{bmatrix} a_0 \\ a_1 \\ a_2 \\ a_3 \\ a_4 \\ a_5 \end{bmatrix} , \qquad (B-8)$$

where a_0 is the zenith TEC, and a_i, $i = 1, 2,...,5$ are the slopes along each of the quintet sector boundaries. The system model is

$$\mathbf{x}_{j+1} = \Phi_j \mathbf{x}_j + \Gamma_j \mathbf{w}_{j+1} \quad . \qquad (B-9)$$

The state transition matrix $\Phi_j = \Phi(t_{j+1}, t_j)$ that predicts the state at t_{j+1}, given the state at t_j, is

$$\Phi = \begin{bmatrix} 1 & 0 & 0 & 0 & 0 & 0 \\ 0 & f & 0 & 0 & 0 & 0 \\ 0 & 0 & f & 0 & 0 & 0 \\ 0 & 0 & 0 & f & 0 & 0 \\ 0 & 0 & 0 & 0 & f & 0 \\ 0 & 0 & 0 & 0 & 0 & f \end{bmatrix} , \qquad (B-10)$$

or

$$\tilde{\mathbf{x}}_{j+1} = \Phi_j \hat{\mathbf{x}}_j \quad . \qquad (B-11)$$

Therefore, the zenith TEC is constant, and $f = e^{-\left(\frac{t_{j+1}-t_j}{\tau}\right)}$ is chosen so that the TEC slope becomes zero after some time. These are the best estimates, in the absence of data, to correct the state estimate. τ is chosen to be 180 min.

The process noise w_i represents ionospheric model uncertainties, and dynamic and stochastic ionospheric effects are excluded from the model. These effects are assumed to be a Gauss-Markov process with zero mean and a variance q_i. Now, each element of the state x_i is assumed to have an uncorrelated and independent Gauss-Markov process. Therefore, Γ is the identity matrix, $\mathbf{I}$ ($\Gamma = \mathbf{I}$).

The predicted state error covariance P depends on Φ, Γ, and Q where Q is the diagonal matrix

$$Q_j = \begin{bmatrix} q_0 & 0 & 0 & 0 & 0 & 0 \\ 0 & q_1 & 0 & 0 & 0 & 0 \\ 0 & 0 & q_2 & 0 & 0 & 0 \\ 0 & 0 & 0 & q_3 & 0 & 0 \\ 0 & 0 & 0 & 0 & q_4 & 0 \\ 0 & 0 & 0 & 0 & 0 & q_5 \end{bmatrix} . \qquad (B-12)$$

The ith element q_i is the variance of the Gauss-Markov process of the ith parameter over the jth interval. q_i is nominally set to 10^{-6}. So the predicted error covariance is

$$\tilde{P}_{j+1} = \Phi_j P_j \Phi_j^T + \Gamma_j Q_{j+1} \Gamma_j^T \quad . \qquad (B-13)$$

The measurement update uses the measurement matrix of partial derivatives:

$$\mathbf{M} = \begin{bmatrix} Z(el_1) & 0 & z_1\left(1 - \dfrac{Az_1 - Az_j}{2\pi/5}\right)Z(el_1) & z_1 \dfrac{Az_1 - Az_j}{2\pi/5} Z(el_1) & 0 & 0 \\ Z(el_2) & . & . & . & . & . \\ Z(el_3) & 0 & 0 & z_3\left(1 - \dfrac{Az_3 - Az_k}{2\pi/5}\right)Z(el_3) & z_3 \dfrac{Az_3 - Az_k}{2\pi/5} Z(el_3) & 0 \\ Z(el_4) & . & . & . & . & . \end{bmatrix} , \qquad (B-14)$$

where $z_1 = \left[\dfrac{\pi/2 - el_j}{\pi/2}\right]^2$, $Az_j < Az_1 < Az_{j+1}$, $z_3 = \left[\dfrac{\pi/2 - el_k}{\pi/2}\right]^2$, $Az_k < Az_3 < Az_{k+1}$, and so on. Now the measurement error covariance R is taken from the computed, smoothed pseudorange error estimates σ_i derived in Equation (B-6) as

$$\mathbf{R} = \begin{bmatrix} \sigma_1 & 0 & 0 & 0 \\ 0 & \sigma_2 & 0 & 0 \\ 0 & 0 & \sigma_3 & 0 \\ 0 & 0 & 0 & \sigma_4 \end{bmatrix} . \qquad (B-15)$$

The measurement update uses a fading memory to allow real changes in the ionosphere to update the model and prevent the consequent filter divergence. The fading memory is implemented by modifying the error covariance by the factor f, as seen in Equation (B-10). The fading memory time constant τ is assumed to be the same as ionosphere decay time (180 min), although there is no physical basis for this assignment. With this formalism, the Kalman gain is

$$\mathbf{K}_j = \tilde{\mathbf{P}}_{j+1}\mathbf{M}_j^T\left[\mathbf{M}_j\tilde{\mathbf{P}}_{j+1}\mathbf{M}_j^T + f\,\mathbf{R}_j\right]^{-1} \quad . \tag{B-16}$$

Then the corrected state estimate is

$$\hat{\mathbf{x}}_{j+1} = \tilde{\mathbf{x}}_{j+1}\mathbf{K}_j\left[\mathbf{y} - \mathbf{M}_j\tilde{\mathbf{x}}_{j+1}\right] \quad , \tag{B-17}$$

and its associated covariance is

$$\hat{\mathbf{P}}_{j+1} = \left(\frac{1}{f}\right)\left[\mathbf{I} - \mathbf{K}_j\mathbf{M}_j\right]\tilde{\mathbf{P}}_{j+1} \quad . \tag{B-18}$$

This sequential estimator has been developed to be data driven and to make few physical assumptions about the ionosphere. It works well under a variety of different conditions. For example, this estimator works well with one or more GPS satellites in view, and it continues to work when the constellation of GPS satellites in view changes. This estimator also seems fairly robust during disturbed ionospheric conditions. Finally, valid recovery of ionosphere parameters was seen even in the presence of selective availability (SA), although there are clearly carrier dither sequences that can defeat the cycle slip detection and correction. This method of estimation can easily be expanded to make use of the following: more parameters, more observations to update the state, the inclusion of a physics-based model for the state transition matrix, and better models for the measurement error covariances and the process noise.

REFERENCES

1. L.E. Thornton (private communication, 1992).
2. J. Sciegienny (private communication, 1991).
3. R. Scott Dahlke, D.S. Coco, and C.E. Coker, "Effect of GPS system biases on differential group delay measurements," ARL-TP-88-17 (August 1988).
4. G.E. Lanyi, T. Roth, and R.E. Neilan, "A comparison of mapped and measured total ionospheric electron content using GPS and beacon satellite observations," in J.M. Goodman, R.G. Klobuchar, and H. Soicher (eds.) *The Effect of the Ionosphere on Communication, Navigation, and Surveillance Systems*, p. 135 (1987).
5. D.S. Coco, C. Coker, S.R. Dahlke, and J.R. Clynch, "Variability of GPS satellite differential group delay biases," *IEEE Trans. Aerosp. Electron. Syst.* **27**, 6, 71-78 (1991).
6. A.J. Coster and E.M. Gaposchkin, "Use of GPS pseudo-range and phase data for measurement of ionospheric and tropospheric refraction," Proc. of *ION GPS-89*, Colorado Springs, Colorado (1989) 439–443.
7. M.J. Buonsanto, "Comparison of incoherent scatter observations of electron density and electron and ion temperature at Millstone Hill with the international reference ionosphere," *J. Atmos. Terr. Phys.* **51**, 5, 441–467 (1989).
8. J.A. Klobuchar, M.J. Bounsanto, M.J. Mendillo, and J.M. Johanson, "The contribution of the plasmasphere to the total time delay," in *The Effect of the Ionosphere on Space and Terrestrial Systems*, ed. J.M. Goodman, Naval Research Laboratory and The Office of Naval Research, Crystal City, Arlington, VA (1978), vol. 2, pp. 486–489.
9. A.J. Coster, E.M. Gaposchkin, L.E. Thornton, M.J. Buonsanto, and D. Tetenbaum, "Comparison of GPS and incoherent scatter measurements of the total electron content," in J.M. Goodman (ed.), *The Effect of the Ionosphere on Radiowave Signals and System Performance*, 460-469, based on Ionospheric Effects Symposium (1–3 May 1990).
10. G. Blewitt, *An Automated Editing Algorithm for GPS Data*, Jet Propulsion Laboratory, Pasadena, Calif., JPL Geodesy and Geophysics Preprint No. 192 (January 1990).
11. A.H. Jazwinski, *Stochastic Processes and Filtering Theory*, New York, New York: Academic Press (1970).
12. E.M. Gaposchkin (private communication, 1992).
13. M.W. Fox, M. Mendillo, and J.A. Klobuchar, "Ionospheric equivalent slab thickness and its modeling applications," *Radio Science* **26**, 2, 429–438 (1991).
14. I.S. Gradshteyn and I.M. Ryzhik, *Table of Integrals, Series, and Products*, ed. 4, New York, New York: Academic Press (1965).

REPORT DOCUMENTATION PAGE

Form Approved
OMB No. 0704-0188

1. AGENCY USE ONLY (*Leave blank*)	2. REPORT DATE	3. REPORT TYPE AND DATES COVERED
	24 August 1992	Technical Report

4. TITLE AND SUBTITLE

Real-Time Ionospheric Monitoring System Using the GPS

5. FUNDING NUMBERS

C — F19628-90-C-0002

6. AUTHOR(S)

Anthea J. Coster, Edward M. Gaposchkin, and Lorraine E. Thornton

7. PERFORMING ORGANIZATION NAME(S) AND ADDRESS(ES)

Lincoln Laboratory, MIT
P.O. Box 73
Lexington, MA 02173-9108

8. PERFORMING ORGANIZATION REPORT NUMBER

TR-954

9. SPONSORING/MONITORING AGENCY NAME(S) AND ADDRESS(ES)

HQ Air Force Materiel Command
AFMC/STSC
Wright-Patterson AFB, OH 45433-5001

10. SPONSORING/MONITORING AGENCY REPORT NUMBER

ESC-TR-91-179

11. SUPPLEMENTARY NOTES

None

12a. DISTRIBUTION/AVAILABILITY STATEMENT

Approved for public release; distribution is unlimited.

12b. DISTRIBUTION CODE

13. ABSTRACT (*Maximum 200 words*)

In satellite tracking using ground-based radars, an estimate of the total electron content (TEC) along the path to the satellite is required to measure the range of the satellite. This estimate is necessary because the radar wave travels at a slower speed as it propagates through the ionosphere. The range error that is introduced is dependent on the radar frequency and on the TEC along the propagation path. The TEC can vary significantly with the time of day, geomagnetic activity, and look direction. A real-time synoptic ionospheric monitoring system has been developed using data acquired from a TI4100 Global Positioning System (GPS) receiver for use at the Millstone Hill satellite-tracking radar. The TI4100 GPS receiver can track up to four GPS satellites at any one time. Each GPS satellite transmits signals at two different L-band frequencies: L1 (1575.42 MHz) and L2 (1227.6 MHz). The TEC along the path to each satellite can be determined by combining both frequencies using the pseudorange and the phase data. The data are input into a Kalman filter that is used to predict the coefficients of a simple TEC model with azimuth and elevation dependence. This model takes advantage of the real-time knowledge provided by the GPS data of the variations in TEC around the Millstone location. The coefficients for this model are then sent to the satellite-tracking computer, and the model is applied in real time to account for the ionospheric path delay to whatever satellite is currently in track. The preliminary results of using this ionospheric monitoring system at Millstone will be discussed. The zenith value of the TEC predicted by our GPS model will be compared with another ionospheric measurement, the foF2 obtained from the collocated University of Lowell Digisonde. The TEC values predicted by our GPS model during both geomagnetically quiet and disturbed time periods will be discussed, as well as those associated with high solar flux time periods. Finally, the improvement in our radar system calibration due to the use of the new GPS model will be demonstrated. This improvement is evident in observations of the average range residual over a pass of the Lageos satellite. The standard deviation of these residuals drops from approximately 20 TEC units to about 5 TEC units when the new GPS model is used to estimate the ionospheric refraction correction. A TEC unit is 10^{16} electrons/m^2. At the Millstone L-band frequency of 1295 MHz, this correction corresponds to an improvement in the standard deviation from 5.3 to 1.4 m. It is our opinion that, outside of upgrading all satellite-tracking radars to dual-frequency capability, the GPS is currently the best monitoring system of the TEC available.

14. SUBJECT TERMS		15. NUMBER OF PAGES
total electron content (TEC) ionospheric model global positioning system (GPS)	ionospheric range delay satellite tracking improvements	40
		16. PRICE CODE

17. SECURITY CLASSIFICATION OF REPORT	18. SECURITY CLASSIFICATION OF THIS PAGE	19. SECURITY CLASSIFICATION OF ABSTRACT	20. LIMITATION OF ABSTRACT
Unclassified	Unclassified	Unclassified	SAR